Weak magnetic field and dense LLVPs: new insights from satellite observations of inner core oscillation

Yachong An[1†], Hao Ding[1†*], Fred D. Richards[2], Weiping Jiang[3*], Jiancheng Li[1*], Wenbin Shen[1]

[1]*School of Geodesy and Geomatics, Hubei LuoJia Laboratory, Wuhan University, 430079, Wuhan, China*

[2]*Department of Earth Science & Engineering, Imperial College London, Royal School of Mines, Prince Consort Road, London, SW7 2AZ, UK*

[3]*GNSS Research Center, Wuhan University, Wuhan, China*

[*]**Corresponding author. Email**: dhaosgg@sgg.whu.edu.cn; wpjiang@whu.edu.cn; jcli@sgg.whu.edu.cn

[†]Y.A. and H.D. contributed equally to this work.

Abstract: The magnetic field within the Earth's core and the density heterogeneity of the large low-velocity provinces (LLVPs) can be theoretically inferred from inner core oscillation via mantle-core coupling mechanisms. However, direct and robust observations of these phenomena remain elusive. While seismological observations have suggested possible evidence for periodic inner core oscillation, the debate continues. In contrast, satellite geodesy provides a new perspective, with decades of global high-precision records. In this study, we independently detect a significant and robust ~6-year inner core oscillation using satellite observations, focusing particularly on the gravitational field Stokes coefficients. This allows us to measure equatorial

topographic undulations of 187±4 m for the first time. By combining this oscillation with the mantle-core gravitational and electromagnetic interaction, we infer a weaker magnetic field within the core (0.3 mT) and a stronger field across the inner core boundary (over 3.2 mT). Additionally, we reveal ~+9‰ mean density anomalies at the base of the dense LLVPs. Our findings reconcile the estimation of internal physical parameters with numerical geodynamo models and offer insights into magnetic field evolution, core motion, and LLVP formation.

Main

The Earth's solid inner core and solid mantle are separated by the liquid outer core[1], and therefore the motions of the inner core are possible relative to the mantle. The motion of the inner core is influenced by the lateral density variation of the lower mantle, as well as by the magnetic field within the core, through both mantle-inner core gravitational (MICG) coupling and electromagnetic coupling[2,3,4].

Early geodynamo simulations predicted a potential slight super-rotation of the inner core relative to the mantle[2], with initial evidence estimated at ~1°/year provided by seismological observations[5]. However, subsequent analyses of seismic wave travel time and the free oscillation modes have presented a mixed picture, suggesting variations in differential rotation ranging from westward to eastward, or even negligible[6-10]. The torque from the MICG coupling is expected to induce an oscillation mode in the differential rotation of the inner core[3,13]. The large low-velocity provinces (LLVPs) are significant sources of the lateral density variation in the lower mantle, extending from the core-mantle boundary (CMB) up to ~1000 km. Both LLVPs exhibit a degree-2, order-2 spherical harmonic $Y_{22}(\Omega)$ spatial structure, characterized by an equatorial antipodal configuration (Fig. 1)[11,12]. If LLVPs are considered as intrinsically dense heterogeneities, the principal axis of the inner core's elliptical equator will align with the principal axis of LLVPs due to the MICG coupling (see as Fig. 1). A slight misalignment could trigger an inner core oscillation mode[3,13]. Rough estimations suggest that the period of inner core oscillation falls within the range of 1-3 years[3], but this period could be greatly prolonged due to electromagnetic coupling[4,14,15]. The magnetic field within the Earth's core and the density of LLVPs remain contentious, as they cannot be directly measured. Proposed decadal-scale torsional waves from Earth's rotation have been linked to sub-millitesla magnetic fields within the core[16,17], whereas recent numerical geodynamo simulations indicate field strengths of 4 mT, ten times stronger than previous estimates[18,19]. Additionally, earlier studies suggested that the density of the Africa and Pacific LLVPs is higher than average[20,21], but this result has been debated because of inherent limitations in the analysis of the relevant data[22]. The mineralogy of the Earth favored a lower-than-average density when modelling seismic wave travel times[23]. Similarly, the Stoneley modes indicate that LLVPs tend to have negative density anomalies, though the possibility of dense at their very base cannot be ruled out[24]. Conversely, tidal tomography suggested a mean excess density anomaly of up to 5-19‰[25]. This leaves the inner core oscillation predicted by the mantle-core interactions still poorly understood. In turn, if inner core oscillation can be detected, it could provide valuable constraints on the magnetic field within the core and density anomalies of the LLVPs.

Seismological observations were regarded as the primary method for gaining insights into the inner core motions, which tended towards the suggestion that the inner core may oscillate relative to the mantle[8,26-29]. Such oscillation could potentially reconcile previously conflicting observations of differential rotation observed during seismic events. Despite this intriguing suggestion, robust evidence for periodic oscillation remains elusive, with proposed oscillation periods vary significantly across different studies. An analysis comparing seismic wave observations at three time points (1969, 1971, 1974) with the length-of-day variation (ΔLOD) attempted to confirm a ~6-year inner core oscillation[27], but this conclusion fails when additional seismic events are considered[29]. Similarly, another study[26] proposed a much longer ~70-year oscillation period, with angular amplitudes reaching ~1.5°, which are significantly higher than those predicted by the dynamic model and free oscillation modes[4,10]. This discrepancy is also attributed to a trap of data selection in recent analyses[28]. Additionally, alternative explanations for the travel time of seismic waves, such as rapid growth of the inner core[30], further contribute to the ongoing controversy and uncertainty surrounding the detection of inner core oscillation.

In addition to changing the travel time of seismic waves[5,7], inner core oscillation can also cause the degree-2 order-2 gravitational field Stokes coefficient variations by driving changes in the Earth's degree-2 order-2 constant density surfaces[3,31] and altering the ΔLOD through the angular momentum exchange with the mantle[3,4]. Here, we will use the gravitational field Stokes coefficients derived from Satellite Laser Ranging

(SRL) (and Gravitational Recovery and Climate Experiment; GRACE) to independently identify periodic signals. We aim to correlate these signals with periodic variations in the ΔLOD to identify a possible inner core oscillation and determine its period and amplitude. These observations will then be used to constrain the core's magnetic field, density anomalies of LLVPs, and the equatorial topographic undulations of the inner core at the inner core boundary (ICB).

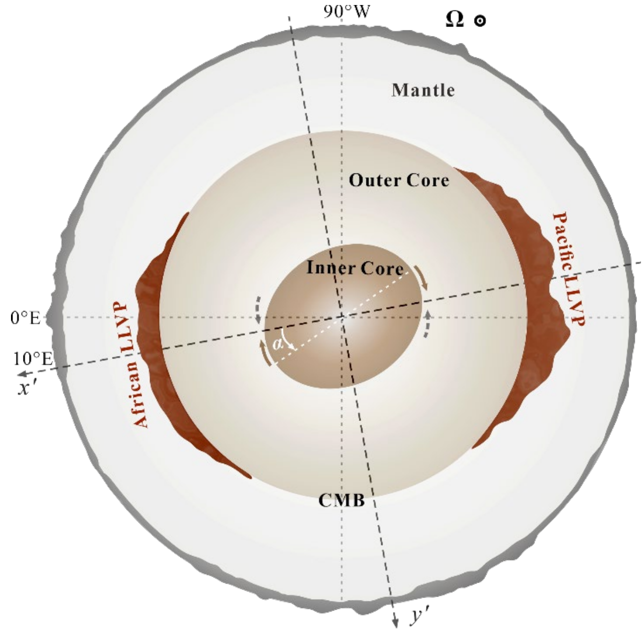

Fig. 1: Inner core oscillation diagram (view from the north pole). The inner core oscillation is a periodic reversal relative to the mantle. The dashed black line is set to the x'-axis in the right-handed coordinate system, representing the principal axis of the LLVPs (10°E-170°W) at the lower mantle. If the density anomalies of the LLVPs are positive, the principal axis of the inner core (dashed white line) will be preferentially aligned with the principal axis of the LLVPs rather than the mantle's figure axis due to stronger gravity. The angle from the principal axis of the LLVPs to the inner core is α due to inner core oscillation.

Results

The angle between the principal axes of the large low-velocity provinces and the inner core

The principal axis of the LLVPs points to ~10°E-10°W[12] as shown in Fig. 1; the inner core will oscillate about this axis due to MICG coupling and will change the ΔLOD due to the angular momentum exchange, so the angle between the principal axes of the LLVPs and the inner core can be inferred from the ΔLOD. The fluctuations in the ΔLOD (1962/1-2020/2) were meticulously corrected using external sources (atmospheric and oceanic effects; Supplementary Fig. 1a), and the hydrological effect is not further considered due to it is far below even the background noise of ΔLOD in the target frequency band (Supplementary Fig. 1b and Supplementary Results). Subsequent removal of tidal effects based on a tidal model[32], a corrected ΔLOD sequence $g_1(t)$ can be obtained (Fig. 2a); and after further employing a 6-month running mean to reduce significant high-frequency noises in the $g_1(t)$, a smoothed ΔLOD sequence $g_2(t)$ is obtained $g_2(t)$ (Fig.2b). The $g_2(t)$ sequence consists of decennial variations and intradecadal (5-year to 10-year) oscillations with an amplitude of ~0.2 ms. Given that the intradecadal variations may be caused by possible inner core motions[14,33,34] while the decadal variations may be caused by fluid core motions[35-37], fluctuations longer than 10-year are fitted and removed using the cosine function and the previously found periods[38] to obtain a final used residual sequence $R(t)$; this process is like that used in Ref. (33). Given the assumption that the $R(t)$ primarily reflects the inner core motion, we can infer the angle α from the principal axes of LLVPs to the inner core, and generating $\varphi(t)$ sequences (Fig. 2b) from $R(t)$ (see Methods).

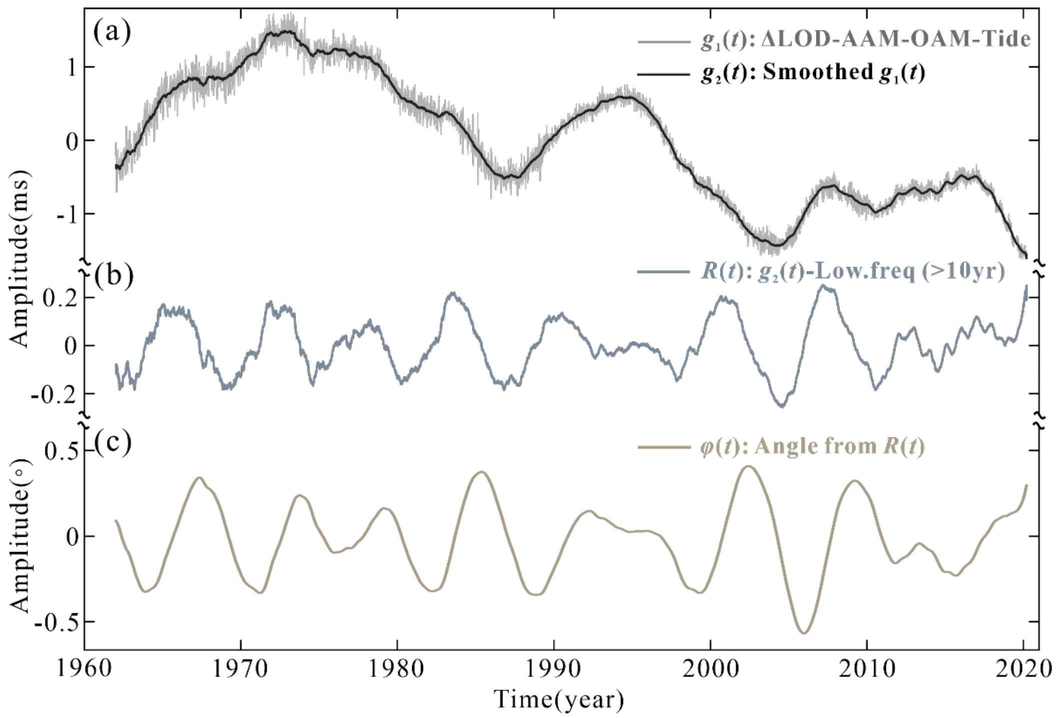

Fig. 2: Angle α from the principal axes of the large low-velocity provinces to inner core inferred from length-of-day variation (ΔLOD) time series. (a) The ΔLOD record with atmospheric and oceanic effects and tide removed ($g_1(t)$ sequences) and smoothed $g_1(t)$ sequences with a 6-month running mean window ($g_2(t)$ sequences). (b) Residual sequence $R(t)$ in which low-frequency signals with a period of more than 10-year are removed from $g_2(t)$ sequences. (c) Angle progression $\varphi(t)$ inferred from $R(t)$.

Searching for the inner core oscillation from the satellite determined Stokes coefficients

Under the mechanism depicted in Fig. 1, the inner core oscillation will also cause variations in the Earth's gravitational field, controlled by the heterogeneous LLVPs of the $Y_{22}(\Omega)$ spatial configuration (also known as quadrupoles). Thus, it is most likely to detect the inner core oscillation from the Stokes coefficient variations ΔC_{22} and ΔS_{22} (see Methods). ΔC_{22} and ΔS_{22} sequences (2002/1-2024/1) determined by SLR (satellite laser ranging) from CSR (recognized products) are firstly corrected using external sources (atmospheric, oceanic, and hydrological effects; AOH effects). Theory predicts that the inner core oscillation can generally cause only observable ΔS_{22} and would not be detected in ΔC_{22} if the LLVPs have the high positive density anomalies as suggested in previous researches[25,39,40] (see Methods). Consequently, we first compare the Fourier power spectra of the ΔC_{22} and ΔS_{22} sequences (Fig. 3a). In the period range of above 2-year, there is only a significant peak corresponding to a ~6-year signal in the spectrum of the ΔS_{22} sequence (Fig. 3a). In contrast to ΔS_{22}, there is a significant spectral peak in the period range of 12-20 years in ΔC_{22}, and a much weaker spectral peak with ~5.3-year period also presents in ΔC_{22}. As the length of the used ΔC_{22} is only 22 years, this spectral peak in the period of 12-20-year is probably not a stationary signal. Given that Fourier spectra are susceptible to non-stationary signals and thus to false results, we re-analyzed these two sequences in Fig. 3b by using the stabilized AR-z methods; this method helps to identify stationary harmonics[41] and has higher frequency resolution than Fourier spectra[42]. Fig. 3b clearly shows a robust ~6-year signal in ΔS_{22} but no corresponding signal in ΔC_{22}, which matches the identifying characteristics of the inner core oscillation. Besides, no significant spectral peak in the period of 12-20 years, which means that the spectral peak in the period of 12-20-year identified in Fig. 3a is not a stationary signal. To verify those results, we also show the Morlet wavelet spectra of the used $\Delta S_{22}/\Delta C_{22}$ after removing the AOH effects (Extended Data Fig. 1); results also show that the ~6-year signal is only present in ΔS_{22}, and limited by period-resolution of the Morlet wavelet spectrum, the 12-20 years oscillation still presents in ΔC_{22} but without a near-fixed period. Additionally, detailed Fourier power spectra of raw data and external excitations for $\Delta C_{22}/\Delta S_{22}$ are presented in Extended Data Fig. 2; we can find that fluctuations observed within the 12-20 years and ~5.3-year periods appear to be influenced by the AOH effects, whereas the ~6-year signal clearly does not come from those effects (Supplementary Results and Extended Data Fig. 2). These findings can be also verified by GRACE data (2002/4-2023/5) and SLR data from the IGG-SLR-HYBRID Ensemble Mean product over a longer time span (1992/11-2020/12) in Supplementary Results, Supplementary Fig. 2 and Supplementary Fig. 3. Based on these results, only a ~6-year signal is the candidate for inner core oscillation, and we refer it as to the SYO (~six-year oscillation). Subsequently, employing the classical least-squares method, we respectively fit the SYOs from ΔS_{22} and the $\varphi(t)$. As Fig 3c shows, the two fitted SYOs demonstrate nearly perfect synchronization. This finding aligns with the theoretical prediction $\Delta S_{22}= \mu\alpha$ (α in °; see Methods), where $\mu= 8.237\times10^{-10}\xi_s > 0$ (ξ_s is a positive triaxiality parameter of the inner core) is obtained from parameters of PREM model. Based on the observed μ of $(5.2\pm0.1)\times10^{-11}$ (derived from Fig. 3c), we estimate the triaxiality parameter ξ_s to be $(6.31\pm0.12)\times10^{-2}$, which is close to the higher value of $\sim6.69\times10^{-2}$ (i.e., the difference in equatorial moments of inertia $B_s-A_s= 9.51\times10^{30}$ kg·m^2) in Ref. (3) inferred from a seismic tomography model of mantle based on the assumption of hydrostatic equilibrium[43]. This consistency strongly supports the assertion that the SYO is just the inner core oscillation. Additionally, the triaxiality parameter ξ_s implies the equatorial topographic undulations of 187±4 m at the ICB.

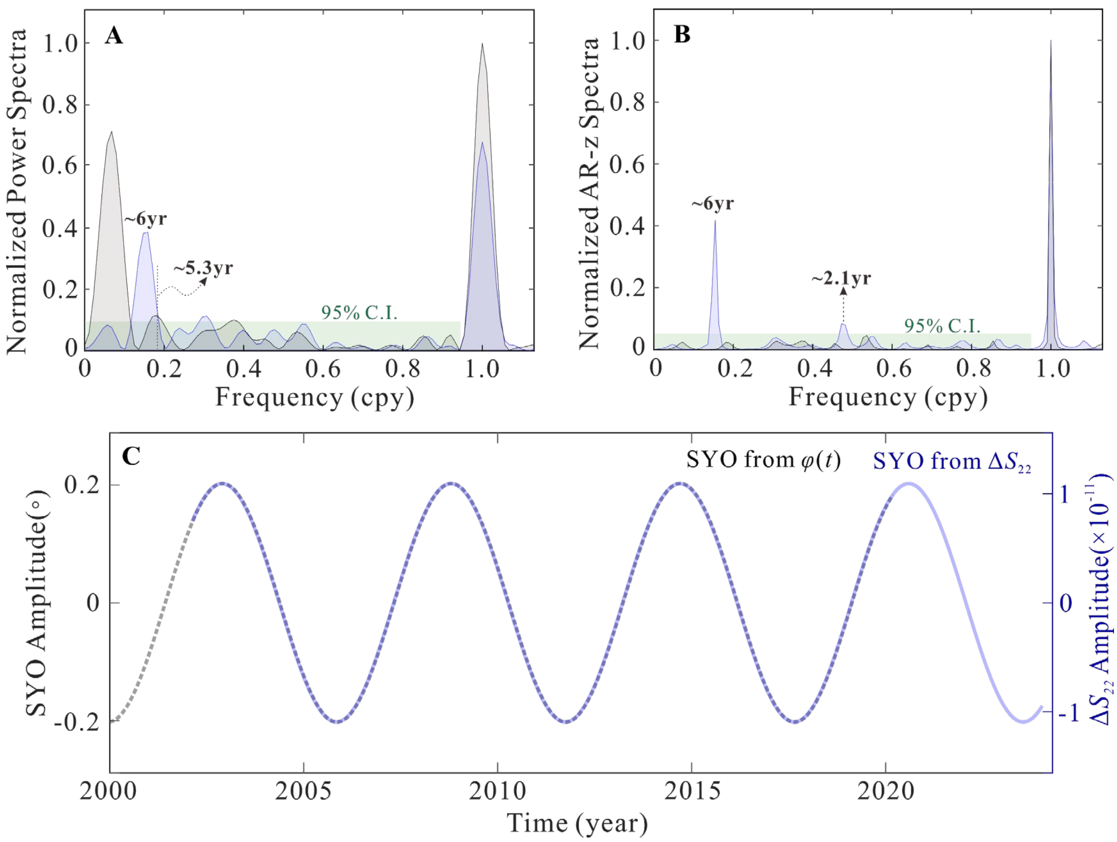

Fig. 3: Verification of the ~6-year oscillation (SYO) for the inner core oscillation from the length-of-day variation (ΔLOD) and degree-2 order-2 Stokes coefficients. (a) The normalized Fourier power spectra of the corrected degree-2 order-2 Stokes coefficient variations ΔC_{22} and ΔS_{22} sequences (2002/1-2024/1) determined by SLR; green region represents the 95% confidence interval (C.I). (b) Similar to (a) but for the stable AR-z spectra. (c) Fitted SYOs from corrected ΔS_{22} sequences and angle $\varphi(t)$ using the classical least-squares method.

Inversion of the magnetic field within the core and density anomalies of the large low-velocity provinces

According to the observed relationship between the ΔS_{22} and the inner core oscillation angle α, we have constrained the parameter ξ_s to the value of $(6.31\pm0.12)\times10^{-2}$. Based on the estimated parameter ξ_s and single significant ~6-year periodic inner core oscillation, it will yield important insights into the magnetic field within the core and density anomalies of LLVPs in the lower mantle.

The magnetic field significantly impacts the period of the inner core oscillation[4,14,15], necessitating the further consideration of electromagnetic coupling to infer the axial gravitational coupling constant from the observed ~6-year period of the inner core oscillation. By action the torque N_s to the inner core (see Methods), the eigen-period of the inner core's axial motion coupled with liquid core can be determined by solving for its angular velocity. Numerical simulations indicate that the uniform magnetic field within the core B_c is constrained to sub-millitesla levels, and the period of inner core oscillation is close to a quasi-decadal. Specifically, with B_c set to 0.3 mT and the axial MICG coupling constant $\hat{\Gamma}_z$ set to 3.7×10^{20} N·m, the theoretical period of the inner core oscillation matches the observed ~6-year. A slight increase in the main period will greatly reduce the coupling constant (see Extended Data Fig. 3), akin to the scenario where the magnetic field is not considered.

The motion of the inner core also excites torsional waves in the liquid core due to electromagnetic coupling[4,14,15], leading to multiple eigen-periods (Extended Data Fig. 3). Leveraging single significant ~6-year signal observed in ΔS_{22}, adjustments are made to the magnetic field across the ICB to suppress wave motions, ensuring the accentuation of the dominant oscillation is accentuated (with the amplitude of any secondary oscillation being at most one-third that of the primary oscillation). For the dominant ~6-year oscillation, numerical simulations show that the core's magnetic field (B_c) is determined to be 0.3 mT, and the field across the ICB exceeds 3.2 mT, corresponding to an axial MICG coupling constant of 3.7×10^{20} N·m. Considering the results from previous studies, the scope is further extended and it requires an axial gravitational coupling constant of $3\times10^{20} < \hat{\Gamma}_z < 4.5\times10^{20}$ N·m if the SYO is the normal mode of inner core oscillation coupled with torsional waves[14,15,33,45]. Then, we obtain an important constraint from 1.59 to 2.48 for the mantle's density multipole of the interior type q_{22}^{M} (see Methods). The mantle's multipole of the interior type q_{22}^{M} can be regarded as weighted $p(a)$ integrals of the density anomaly $\varepsilon_{22}(a)$ of the bodies with spherical harmonic $Y_{22}(\Omega)$ spatial structure over the entire mantle. As depicted in Fig. 4a, the weight $p(a)$-curve diminishes as the mean radius a increases, indicating a strong constraint on the degree-2 order-2 density anomaly in the lower mantle (blue and red dotted areas in Fig. 4b), corresponding to the highly heterogeneous and controversial density of the LLVPs for q_{22}^{M}. Thus, q_{22}^{M} can be used to constrain the density anomalies of the LLVPs.

Next, we use the constraint and the seismic shear wave speed (v_s) model of the mantle to invert the density anomalies of the LLVPs. The perturbation in shear wave speed v_s is converted perturbations in density ρ (i.e., density anomalies) by the $R_\rho = \partial\ln\rho/\partial\ln v_s$[25,46]. In the upper mantle and the middle and upper layers of the lower mantle (depth 0-1801 km), density anomalies are from the converted perturbations in seismic velocities based on the scaling factors from Ref (46). In the middle and lower layers of the lower mantle (depth 1801-2891 km), different seismic tomographic models show that the LLVPs have similar long-wavelength structure[25], especially the spatial distribution of spherical harmonic $Y_{22}(\Omega)$. Since the S40RTS[47] and S362MANI[48] models are sensitive to the LLVPs[25], we mainly adopted them to invert perturbations in density ρ. For the basalt in the deepest 100-200 km of the LLVPs, there may be a primitive chemical reservoir[40], as a constant R_ρ conversion is used from CMB to a depth of 2691 km. In the outermost layer of the LLVPs (depth 1801-2131 km), the density anomalies are obtained by setting $R_\rho = 0.2$ from Refs. (25) and (46). To smooth the transition of density to the upper and middle layers of the lower mantle, the R_ρ is varied linearly with depth from 2131 to 2691 km. The density anomalies of the LLVPs are obtained by adjusting R_ρ and applying crust correction based on the model CRUST1.0[49] to meet the multipole constraint q_{22}^{M}. Fig. 4a shows the variation of the mean density anomalies with radius of the deep LLVPs below the radius and the contour of the LLVPs in each layer (see green curves in Fig. 4b) is defined by the −6.5‰ V_s[25,40,46] based on the S40RTS model (similar results based on the S362MANI model are shown in Extended Data Fig. 4). For the bottom two-thirds of the LLVPs, the mean density of our inversion is +4.5-5.8‰ higher than that of the surroundings based on the S40RTS model (+4.7-6.1‰ for S362MANI model), consistent with the independent result of +5‰ constrained by the tidal tomography[25]. Fig. 4b shows the density anomalies of the layer at the depth of 2851 km (40 km from the CMB; mean radius a= 3520 km) based on the constraint of density multipole $q_{22}^{\mathrm{M}} = 2.16$ (corresponding to the axial gravitational torque of $\hat{\Gamma}_z = 4.0\times10^{20}$ N·m)[15] and S40RTS model; this indicates the very dense LLVPs at the bottom with a mean density anomaly of about ~+9‰, which is close to the independent result (~+10‰) of Stoneley mode splitting functions[24]. These independent measurements corroborate each other and indicate that LLVPs have large positive density anomalies and that there may indeed be an abnormally dense layer at the bottom[24,25,39,40]. More importantly, these conformities in turn support ~6-year signal for the inner core oscillation.

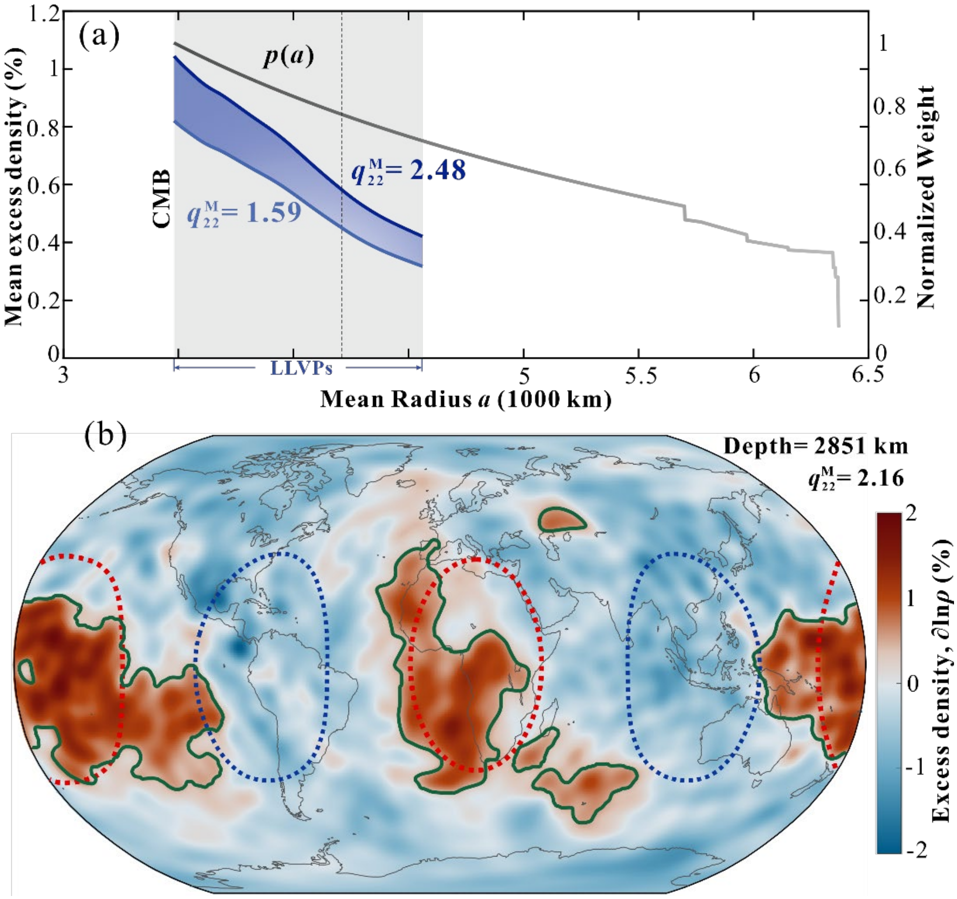

Fig. 4: Inversion of the density anomaly of the large low-velocity provinces (LLVPs) based on S40RTS model. (a) Normalized weight function $p(a)$ (gray curve) and the mean radius-dependent mean density anomaly range of the LLVPs below the radius (blue shaded area); the gray shaded area indicates the LLVPs location range. (b) The excess density $\partial \ln\rho$ (in %) converted by the S40RTS model at the depth of 2851 km is based on the mantle's interior multipole value of 2.16 (corresponding to the axial gravitational torque of 4.0×10^{20} N·m); the green curves circle the contour of the LLVPs defined by the $-6.5‰ V_s$; the dashed curves circle the sensitive region of degree-2 order-2 density multipoles and different colors mean that they have opposite symbols.

Discussion

Growing evidence suggests that the equatorial plane of the inner core is elliptical[3,43,50], shaped by lateral differences in the lowermost mantle density due to the LLVPs. Under this premise, if the inner core exhibits stable super-rotation, periodic oscillation would be nearly impossible because the physical mechanism would rapidly degrade unless the inner core has low viscosity and can deform viscously[51]. However, different observations have shown that inner core oscillation is not only possible but also persistent, potentially driven by gravitational coupling between the inner core and the LLVPs in the lower mantle[3,13-15,44]. While seismology provides a traditional means of probing the inner core motions, it suffers from limitations such as sparse seismic events coverage[5,26-29] and ambiguity in interpreting different travel times of seismic waves[30]. In contrast, to verify the existence of inner core oscillation (and determine its period), we use high-precision, low-degree satellite gravitational field data as a new observational constraint. This data offers high temporal resolution (monthly sampling) and reflects the overall change in the inner core's equatorial plane, avoiding data selection biases[28] and the influence of rapid inner core growth in seismology[30].

Theoretical analysis suggests that inner core oscillation should manifest only in the gravitational field coefficient ΔS_{22} and not in ΔC_{22} based on the assumption that LLVPs are dense. Our measurements confirm this, showing a ~6-year signal exclusively in ΔS_{22}, aligning with theoretical predictions. Correspondingly, there is also an SYO in the ΔLOD. Since the signal in the ΔLOD is caused by the exchange of angular momentum between Earth's different layers, after excluding possible external sources, it is currently considered to be most likely to originate from inner core oscillation. Furthermore, the SYO in ΔS_{22} corresponds well in phase to that in the inner core differential rotation angle inferred from ΔLOD (this is also consistent with the verification based on seismic waves in Ref. (27)). This finding further confirms that the SYO is from inner core oscillation and that the gravitation coupling between the inner core and LLVPs plays a key role in its mechanism.

By integrating satellite geodesy observations with theoretical analysis, we estimate the inner core's triaxiality as $(6.31\pm0.12)\times10^{-2}$; this means that the inner core's equatorial topographic undulations of 187±4 m and a difference in equatorial inertia moments B_s-A_s of $(8.972\pm0.172)\times10^{30}$ kg·m^2, aligning closely with the high value inferred from seismic tomography[3,43]. The magnetic field in the liquid core will further complicate the motion, leading to multiple periods and extending the main period. According to the observed single significant ~6-year oscillation, we determine a core magnetic field of 0.3 mT and a field across the ICB exceeding 3.2 mT, with the axial MICG coupling constant range from 3×10^{20} N·m to 4.5×10^{20} N·m. Based on the axial MICG coupling constant and inner core's equatorial topographic undulations, we further inverted very dense LLVPs at their base with a mean density anomaly of ~+9‰, and the bottom two-thirds of the two LLVPs with the mean density anomaly of +4.5-5.8‰, which agree with independent measurements from Stoneley mode splitting function and tidal tomography[24,25,40], respectively. This coherence across multiple lines of observed evidence not only strengthens the argument for the proposed mechanism of ~6-year inner core oscillation but also underscores the intricate interplay between

Earth's inner core, magnetic field, and mantle dynamics. Collectively, these findings from satellite geodesy make contribute significantly to our comprehension of the Earth's inner core structure and the dynamic processes governing its behavior.

Materials and Methods

Inferring the angle α from the length-of-day variation

In the MICG coupling system, the relationship between the mantle angular velocity variation $\Delta\omega_m$ and the inner core angular velocity variation $\Delta\omega_s$ is established through

$$\Delta\omega_s C_s = -\Delta\omega_m C_m \tag{1}$$

where C_s= 5.8673×10^{34} kg·m^2 and C_m= 7.1236×10^{37} kg·m^2 are the axial inertia moments of the inner core and mantle, respectively. The angular velocity variation of the mantle can be obtained from the observed ΔLOD by

$$-\frac{\Delta\omega_m}{\Omega_0} = \frac{\Delta\mathrm{LOD}}{\mathrm{LOD}} \tag{2}$$

where LOD= 86400 s, and Ω_0 denotes the mean sidereal rotation rate. The rotated angle of the mantle in the opposite direction is negligible compared to the rotated angle of the inner core, and the angle α is

$$\alpha = \int \Delta\omega_s \mathrm{d}t \tag{3}$$

Eqs. (1)-(3) yield the final expression of the angle α

$$\alpha = \frac{C_m}{C_s}\frac{\Omega_0}{\mathrm{LOD}}\int \Delta\mathrm{LOD}\mathrm{d}t \tag{4}$$

In inverting the angle α, we assume that the ΔLOD is caused by the inner core oscillation or super-rotation, which is valid for a certain frequency band.

Changes in Stokes coefficients caused by the inner core oscillation

The inner core oscillation causes the misalignment of the mantle and inner core in the equatorial plane, which is associated with degree-2 order-2 ellipticity and further causes a change in the Earth's gravity field. Thus, only the degree-2 order-2 ellipticity of the Earth needs to be considered, and constant density surfaces of Earth are written as[3]

$$r' = a\left(1+\epsilon' Y_{22} + \epsilon'^{*} Y_{2-2}\right) \tag{5}$$

where $\epsilon' = \epsilon'(a)$ denotes the equatorial ellipticity varying with mean radius a, the asterisk '*' represents complex conjugation, and $Y_{22} = Y_{22}(\theta, \varphi)$ is degree-2 order-2 fully normalized spherical harmonic function. Given that the selected x'-axis aligns with the principal axes of the inner core and LLVPs in static equilibrium, the ellipticity ϵ' can be approximated as a real number.

The inner core oscillation only involves rotation in the equatorial direction. Following an equatorial rotation in the longitudinal direction α, as shown in Fig. 1, the elastic displacement in constant density surfaces of the inner core caused by the misalignment of the inner core is

$$\Delta\hat{r}_s = \hat{r}_s - r' = (1+h_{\epsilon'})(\tilde{r}_s' - r_s') = \sum_{m=-2}^{2} \gamma_\alpha^m a\epsilon'\left(1+h_{\epsilon'}\right) Y_{2m} \tag{6}$$

where

$$\begin{aligned} \gamma_\alpha^0 &= \gamma_\alpha^{\pm 1} = 0 \\ \gamma_\alpha^{\pm 2} &= e^{\mp i2\alpha} - 1 = \mp i2\alpha \end{aligned} \tag{7}$$

Similar to the inner core wobble, we only need to replace the ellipticity ϵ and $\delta_{\beta\alpha}^{m}$ in

Ref. (43) with ϵ_{22} and γ_α^m, respectively, to derive the conclusion regarding inner core oscillation. Thus, the change in the surface's gravitational field caused by the elastically misaligned inner core is

$$\Delta U(a_e,\theta,\lambda) = G\sum_{m=-2}^{2}\gamma_\alpha^m\sqrt{\frac{4\pi}{5}}\frac{1}{a_e^3}\left(\mathcal{H}_{s'} - \mathcal{H}_{s'}'\right)\left[1+\tilde{k}_{\epsilon'}(a_e)\right]Y_{2m} \tag{8}$$

where G= 6.672×10^{-11} N·m^2·kg^{-2} denotes gravitational constant, a_e= 6.371×10^6 m represents the mean radius of the Earth, and the factor $[1+\tilde{k}_{\epsilon'}(a_e)]$= 1.9736 accounts for the Earth's elastic deformations associated with the density change at the ICB and is written as[52]

$$\tilde{k}_{\epsilon'}(a_e) = \frac{\mathcal{H}^{\epsilon'}}{\left(\mathcal{H}_{s'} - \mathcal{H}_{s'}'\right)} \tag{9}$$

Those three parameters related to equatorial ellipticity are defined as

$$\mathcal{H}_{s'} = -\sqrt{\frac{4\pi}{5}}\int_0^{a_s}\rho\frac{\mathrm{d}(a^5\epsilon')}{\mathrm{d}a}\mathrm{d}a \tag{10a}$$

$$\mathcal{H}_{s'}' = -\sqrt{\frac{4\pi}{5}}\int_0^{a_s}\rho_f'\frac{\mathrm{d}(a^5\epsilon')}{\mathrm{d}a}\mathrm{d}a \tag{10b}$$

$$\mathcal{H}^{\epsilon'} = -\sqrt{\frac{4\pi}{5}}\int_0^{a_e}\rho\frac{\mathrm{d}(a^5 h_\epsilon \epsilon')}{\mathrm{d}a}\mathrm{d}a \tag{10c}$$

where a_s= 1.2215×10^6 m denotes the mean radius of the ICB. The triaxiality parameter of the inner core is also used here, and it is defined as

$$\xi_s = \frac{B_s - A_s}{C_s - \frac{A_s + B_s}{2}} = -4\sqrt{\frac{1}{6}}\int_0^{a_s}\rho\frac{\mathrm{d}(a^5\epsilon')}{\mathrm{d}a}\mathrm{d}a \Big/ \int_0^{a_s}\rho\frac{\mathrm{d}(a^5\epsilon)}{\mathrm{d}a}\mathrm{d}a \tag{11}$$

where B_s and A_s denote the equatorial principal moments of inertia of the inner core, respectively, arranged in descending order. Since the inner core's density changes very little (only ~2.5% from the Earth's center to the ICB based on the PREM model[1]), the two unknown quantities in Eqs. 10a and 10b are linked to the known quantities defined in Ref. (52) based on the triaxiality parameter,

$$\mathcal{H}_{s'} = -\frac{\sqrt{6}}{4}\xi_s \mathcal{H}_s \tag{12a}$$

$$\mathcal{H}_{s'}' \approx -\frac{\sqrt{6}}{4}\xi_s \mathcal{H}_s' \tag{12b}$$

The error introduced by the approximation of Eq. 12b is negligible, and can therefore be equated. Based on the PREM model[1], we can calculate the parameters $\mathcal{H}_s$= 1.418×10^{32} kg·m^2 and $\mathcal{H}_s'$= 1.342×10^{32} kg·m^2. The inner core oscillation only causes the degree-2 order-2 Stokes coefficient change, and considering the difference between geographic coordinate and set in this study, it is written as

$$\begin{aligned}\Delta C_{22} + i\Delta S_{22} &= i\sqrt{\frac{3}{5}}\frac{1}{Ma_e^2}\xi_s\left(\mathcal{H}_s - \mathcal{H}_s'\right)\left[1+\tilde{k}_{\epsilon'}(a_e)\right]e^{-i\frac{10^\circ}{180^\circ}\pi}\alpha \\ &\equiv (\upsilon + i\mu)\alpha\end{aligned} \tag{13}$$

If the density anomalies of the LLVPs are positive, it will be likely that the inner oscillation only causes the observable ΔS_{22}. Otherwise, it will cause observable changes in ΔC_{22}. Based on the above parameters, it can be calculated μ= $8.237\times10^{-10}\xi_s$ (where α is in °).

The axial gravitational torsion constant and period of inner core oscillation with magnetic field

In the MICG coupling system, the liquid core acts only as a pressure on the inner core. In fact, there is a strong magnetic field in the core, especially at the ICB, resulting in electromagnetic coupling between the solid core and liquid core. Under the action of electromagnetic torque, the inner core will couple with the nearby liquid core and excite torsional waves in the core[4,14,15]. This is not expected to change the gravity conclusions described above, but it will significantly change the period of the inner core oscillation[4,14,15]. Therefore, modeling of electromagnetic torque and torsional waves in the core is necessary to infer the axial gravitational torsion constant from the observed period of the inner core oscillation. Fluid motion within the tangent cylinder of the inner core approximates rigid body rotation due to strong electromagnetic coupling at the ICB[14,53,54]. Compared with topographic coupling and viscous coupling, electromagnetic coupling at the ICB is strongest, ignoring other boundary layer coupling for simplicity, the frequency domain form of the governing equation of the angular velocity can be approximated as[14]

$$\mathrm{M}\begin{bmatrix} u_c \\ u_s \\ u_m \end{bmatrix} = \begin{bmatrix} 0 \\ N_s \\ 0 \end{bmatrix} \tag{14a}$$

where u_c is the effective angular velocity of the tangential cylinder rotating nearly rigidly, u_s and u_m are the angular velocities of the core and mantle, respectively, and N_s is the random torque applied to the inner core, set here to 1×10^{18} N·m. M is a coefficient matrix of the form

$$\mathrm{M} = \begin{bmatrix} \alpha + \omega\hbar\left(\frac{\omega}{|\omega|} - i\right) - \omega^2 C_c & -\omega\hbar\left(\frac{\omega}{|\omega|} - i\right) & 0 \\ -\omega\hbar\left(\frac{\omega}{|\omega|} - i\right) & \hat{\Gamma}_z + \omega\hbar\left(\frac{\omega}{|\omega|} - i\right) - \omega^2 C_s & -\hat{\Gamma}_z \\ 0 & -\hat{\Gamma}_z & \hat{\Gamma}_z - \omega^2 C_m \end{bmatrix} \tag{14b}$$

where α is the frequency-dependent term denoted by

$$\alpha = \frac{1}{2}\tau'(a_s) - \tau(a_s) H(a_s, a_p) \tag{15a}$$

$\tau(a_s)$ denotes the magnetic tension between adjacent cylinders at the ICB, sign prime represents the derivation of the distance s from the rotation axis, and the magnetic tension at s is[14,15]

$$\tau(s) = \frac{4\pi\{B_s^2\}}{\mu_0} s^3 \left(a_f^2 - s^2\right)^{1/2} \tag{15b}$$

where a_f= 3.480×10^6 m denotes the mean radius of the CMB; B_s is the s component of the magnetic field and braces indicate the average over the cylindrical surface. For simplicity, a uniform magnetic field is adopted ($\{B_s^2\} = B_c^2$). The $H(a_s, a_p)$ also depends on the frequency of the oscillation and is expressed as[24]

$$\begin{aligned} H\left(a_s, a_p\right) = -i\frac{\omega}{c} + \frac{1}{2}\left\{u_b'(a_p)/u_b(a_p) + \left[\frac{\tau'(a_p)}{2\tau(a_p)} + \frac{i\omega}{c}\right]\right\} \\ \left\{\exp\left[2i\frac{\omega}{c}\left(a_s - a_p\right)\right] + 1\right\}\left\{\exp\left[2i\frac{\omega}{c}\left(a_s - a_p\right)\right] - 1\right\}^{-1} \\ \left\{1 + \frac{c}{2i\omega}\left\{u_b'(a_p)/u_b(a_p) + \left[\frac{\tau'(a_p)}{2\tau(a_p)} + \frac{i\omega}{c}\right]\right\}\right\}^{-1} \end{aligned} \tag{15c}$$

where c denotes the wave speed, approximately constant in a uniform magnetic field, written as

$$c = \sqrt{\frac{\{B_s^2\}}{\mu_0 \bar{\rho}_f}} \tag{15d}$$

where μ_0= 4π×10^{-7} Wb·(A·m)$^{-1}$ is the vacuum permeability, and $\bar{\rho}_f$ = 1×10^4 kg·m^{-3} is the average density of the core[37,48]. The two approximate analytical solutions for the angular velocity of the fluid and their at a_p derivative are continuous. $u_b(s)$ denotes the angular velocity of the fluid near the CMB, and the relation between its derivative and the angular velocity at a_p is

$$u_b'(a_p) = -\frac{2}{3}\frac{\omega^2}{c^2}\left(a_p - a_f\right) / \left(1 - \frac{1}{3}\frac{\omega^2}{c^2}\left(a_p - a_f\right)^2\right) u_b(a_p) \tag{15e}$$

Thus, $u_b(a_p)$ can be eliminated in Eq. 15c by Eq. 15e. Besides, $\hbar$ in the coefficient matrix M is a function of the electromagnetic coupling strength at the ICB, which is expressed as[14,15,51]

$$\hbar = \frac{2}{3}\pi B_{\mathrm{ICB}}^2 \sigma_f \delta_f a_s^4 \tag{15f}$$

B_{ICB} is the magnetic field strength at the ICB, $\sigma_f = 5\times10^5$ S·m^{-1} is the conductivity of the core, δ_f is the magnetic skin depth, which depends on frequency and conductivity, and $\delta_f = 9.8$ km for the ~6-year period signal in the core.

The axial gravitational torsion constant and density multipoles

After determining the triaxiality parameter of the inner core, the density multipole of the mantle can be inverted utilizing the axial gravitational torsion constant, provided the SYO corresponds to the inner core oscillation. The axial gravitational torsion constant is mainly contributed by degree-2 order-2 density multipoles and is expressed as[13,55-57]

$$\hat{\Gamma}_z = \frac{32\pi}{5} G\gamma f_s \left|q_{22}^{\mathrm{M}}\right| \left|Q_{22}^{s}\right| \tag{16}$$

where the factor $\gamma = \Delta\rho/\rho_s = 0.0468$ accounts for the hydrostatic pressure effect of the passive outer core, and the factor $f_s = 0.85$ account for elastic deformation of the inner core oscillation[13,55,57]. The degree-2 order-2 multipole of the interior type belonging to the mantle q_{22}^{M} and the exterior type belonging to the inner core Q_{22}^{s} are defined as[13,57]

$$q_{22}^{\mathrm{M}} = \iiint_{\mathrm{Mantle}} \rho(\mathbf{r}) r^{-1} Y_{22}(\Omega) \mathrm{d}r\mathrm{d}\Omega \tag{17a}$$

$$Q_{22}^{s} = \iiint_{\mathrm{IC}} \rho(\mathbf{r}) r^{4} Y_{22}^{*}(\Omega) \mathrm{d}r\mathrm{d}\Omega \tag{17b}$$

respectively. An alternative idea to Eq. 5 is to consider the 3-D density of the Earth, similarly focusing only on the degree-2 order-2 lateral variation of the Earth, the density is expressed as[13,57]

$$\rho(r,\theta,\varphi) = \rho_{\mathrm{Model}}(r)\left(1 + \varepsilon_{22}Y_{22} + \varepsilon_{22}^{*}Y_{2-2}\right) \tag{18}$$

where ε_{22} denotes the density anomaly coefficient of the spherical harmonic $Y_{22}(\theta, \varphi)$. Using Eq. 18, Eqs. 17a and 17b can be re-written as

$$\begin{aligned} q_{22}^{\mathrm{M}} &= \int_{a_f}^{a_e} \frac{\rho_{\mathrm{Model}}(a)\varepsilon_{22}(a)}{a}\mathrm{d}a \\ &= \int_{a_f}^{a_e} p(a)\varepsilon_{22}(a)\mathrm{d}a \end{aligned} \tag{19a}$$

$$\begin{aligned} Q_{22}^{s} &= \int_{0}^{a_s} a^{4}\rho_{\mathrm{Model}}(a)\varepsilon_{22}^{*}(a)\mathrm{d}a \\ &= \sqrt{\frac{15}{32\pi}}(B_s - A_s)\exp(-2i\Lambda) \\ &= \sqrt{\frac{15}{32\pi}}\xi_s C_s e_s \exp(-2i\Lambda) \end{aligned} \tag{19b}$$

where $p(a)$ is defined as the weight function of density anomaly coefficient in the mantle, and we can discern what part q_{22}^{M} is sensitive to by analyzing the weight function $p(a)$-curve in the mantle; Λ represents the angle between the direction of the minimum moment of inertia of the inner core A_s and the x-axis of geographical coordinate; $e_s = 2.422\times10^{-3}$ denotes the dynamical ellipticity of the inner core. By combining Eqs. 16 and 19, we obtain the final relation

$$\left|q_{22}^{\mathrm{M}}\right| = \sqrt{\frac{5}{96\pi}}\frac{\hat{\Gamma}_z}{G\gamma f_s \xi_s C_s e_s} \tag{20}$$

References

1. Dziewonski, A. M. & Anderson, D. L. Preliminary reference Earth model. *Phys. Earth Planet. Inter.* **25**, 297-356 (1981).

2. Gubbins, D. Rotation of the inner core. *J. Geophys. Res. Solid Earth* **86**, 11695-11699 (1981).

3. Buffett, B. A. Gravitational oscillations in the length of day. *Geophys. Res. Lett.* **23**, 2279-2282 (1996).

4. Buffett, B. A. A mechanism for decade fluctuations in the length of day. *Geophys. Res. Lett.* **23**, 3803-3806 (1996).

5. Song, X. & Richards, P. G. Seismological evidence for differential rotation of the Earth's inner core. *Nature* **382**, 221-224 (1996).

6. Creager, K. C. Inner core rotation rate from small-scale heterogeneity and time-varying travel times. *Science* **278**, 1284-1288 (1997).

7. Vidale, J. E., Dodge, D. A. & Earle, P. S. Slow differential rotation of the Earth's inner core indicated by temporal changes in scattering. *Nature* **405**, 445-448 (2000).

8. Tkalčić, H., Young, M., Bodin, T., Ngo, S. & Sambridge, M. The shuffling rotation of the Earth's inner core revealed by earthquake doublets. *Nat. Geosci.* **6**, 497-502 (2013).

9. Deuss, A. Heterogeneity and anisotropy of Earth's inner core. *Annu. Rev. Earth Planet. Sci.* **4**, 103-126 (2014).

10. Laske, G. & Masters, G. Limits on differential rotation of the inner core from an

analysis of the Earth's free oscillations. *Nature* **402**, 66-69 (1999).

11. Conrad, C. P., Steinberger, B. & Torsvik, T. H. Stability of active mantle upwelling revealed by net characteristics of plate tectonics. *Nature* **498**, 479-482 (2013).

12. Dehant, V., Campuzano, S. A., De Santis, A. & van Westrenen, W. Structure, materials and processes in the Earth’s core and mantle. *Surv. Geophys.* **43**, 263-302 (2022).

13. Chao, B. F. Dynamics of axial torsional libration under the mantle-inner core gravitational interaction. *J. Geophys. Res. Solid Earth* **122**, 560-571 (2017).

14. Mound, J. E. & Buffett, B. A. Interannual oscillations in length of day: Implications for the structure of the mantle and core. *J. Geophys. Res. Solid Earth* **108**, 2334 (2003).

15. Buffett, B. A. & Mound, J. E. A Green's function for the excitation of torsional oscillations in the Earth's core. *J. Geophys. Res. Solid Earth* **110**, B08104 (2005).

16. Zatman, S. & Bloxham, J. Torsional oscillations and the magnetic field within the Earth's core. *Nature* **388**, 760-763 (1997).

17. Buffett, B. A., Mound, J. E. & Jackson, A. Inversion of torsional oscillations for the structure and dynamics of Earth's core. *Geophys. J. Int.* **177**, 878-890 (2009).

18. Aubert, J., Labrosse, S. & Poitou, C. Modelling the palaeo-evolution of the geodynamo. *Geophys. J. Int.* **179**, 1414-1428 (2009).

19. Gillet, N., Jault, D., Canet, E. & Fournier, A. Fast torsional waves and strong magnetic field within the Earth’s core. *Nature* **465**, 74-77 (2010).

20. Ishii, M. & Tromp, J. Normal-mode and free-air gravity constraints on lateral

variations in velocity and density of Earth's mantle. *Science* **285**, 1231-1236 (1999).

21. Ishii, M. & Tromp, J. Even-degree lateral variations in the Earth's mantle constrained by free oscillations and the free-air gravity anomaly. *Geophys. J. Int.* **145**, 77-96 (2001).

22. Romanowicz, B. The buoyancy of Earth's deep mantle. *Nature* **551**, 308-309 (2017).

23. Schuberth, B. S., Zaroli, C. & Nolet, G. Synthetic seismograms for a synthetic Earth: long-period P-and S-wave traveltime variations can be explained by temperature alone. *Geophys. J. Int.* **188**, 1393-1412 (2012).

24. Koelemeijer, P., Deuss, A., & Ritsema, J. Density structure of Earth's lowermost mantle from Stoneley mode splitting observations. *Nat. Commun*. **8**, 15241 (2017).

25. Lau, H. C., Mitrovica, J. X., Davis, J. L., Tromp, J., Yang, H. Y., & Al-Attar, D. Tidal tomography constrains Earth's deep-mantle buoyancy. *Nature* **551**, 321-326 (2017).

26. Yang, Y., & Song, X. Multidecadal variation of the Earth's inner-core rotation. *Nat. Geosci.* **16**, 182-187 (2023).

27. Wang, W., & Vidale, J. E. Seismological observation of Earth's oscillating inner core. *Sci. Adv.* **8**, eabm9916 (2022).

28. Tkalčić, H. On the inner-core differential-rotation (un) resolvability from earthquake doublets: The traps of data selection. *Geophys. Res. Lett.*, **51**, e2023GL107043 (2024).

29. Wang, W., Vidale, J. E., Pang, G., Koper, K. D. & Wang, R. Inner core backtracking

by seismic waveform change reversals. *Nature* **631**, 340-343 (2024).

30. Wen, L. Localized temporal change of the Earth's inner core boundary. *Science* **314**, 967-970 (2006).

31. Dumberry, M., & Mandea, M. Gravity variations and ground deformations resulting from core dynamics. *Surv. Geophys.* **43**, 1-35 (2022).

32. Ray, R. D., & Erofeeva, S. Y. Long-period tidal variations in the length of day. *J. Geophys. Res. Solid Earth* **119**, 1498-1509 (2014).

33. Holme, R., & De Viron, O. Characterization and implications of intradecadal variations in length of day. *Nature* **499**, 202-204 (2013).

34. Gross, R. S. Earth rotation variations-long period. *Treatise on Geophysics* **3**, 239-294 (2007).

35. Braginsky, S. I. Magnetic Rossby waves in the stratified ocean of the core, and topographic core-mantle coupling. *Earth, Planets. Space*. **50**, 641-649 (1998).

36. Braginsky, S. I. Dynamics of the stably stratified ocean at the top of the core. *Phys. Earth Planet. Inter.* **111**, 21-34 (1999).

37. Buffett, B. Geomagnetic fluctuations reveal stable stratification at the top of the Earth's core. *Nature* **507**, 484-487 (2014).

38. Ding, H. Attenuation and excitation of the ~6 year oscillation in the length-of-day variation. *Earth Planet. Sci. Lett.* **507**, 131-139 (2019).

39. Yuan, Q., Li, M., Desch, S. J., Ko, B., Deng, H., Garnero, E. J., ... & Asimow, P. D. Moon-forming impactor as a source of Earth's basal mantle anomalies. *Nature* **623**, 95-99 (2023).

40. Richards, F. D., Hoggard, M. J., Ghelichkhan, S., Koelemeijer, P. & Lau, H. C. Geodynamic, geodetic, and seismic constraints favour deflated and dense-cored LLVPs. *Earth Planet. Sci. Lett.* **602**, 117964 (2023).

41. Ding, H., Pan, Y., Xu, X. Y., Shen, W. & Li, M. Application of the AR-z spectrum to polar motion: A possible first detection of the inner core wobble and its implications for the density of Earth's core. *Geophys. Res. Lett.* **46**, 13765-13774 (2019).

42. Ding, H. & Chao, B. F. Application of stabilized AR-z spectrum in harmonic analysis for geophysics. *J. Geophys. Res. Solid Earth* **123**, 8249-8259 (2018).

43. Forte, A. M., Woodward, R. L. & Dziewonski, A. M. Joint inversions of seismic and geodynamic data for models of three-dimensional mantle heterogeneity. *J. Geophys. Res. Solid Earth* **99**, 21857-21877 (1994).

44. Mound, J. E. & Buffett, B. A. Detection of a gravitational oscillation in length-of-day. *Earth Planet. Sci. Lett.* **243**, 383-389 (2006).

45. Davies, C. J., Stegman, D. R. & Dumberry, M. The strength of gravitational core-mantle coupling. *Geophys. Res. Lett.* **41**, 3786-3792 (2014).

46. Karato, S. I. Importance of anelasticity in the interpretation of seismic tomography. *Geophys. Res. Lett.* **20**, 1623-1626 (1993).

47. Ritsema, J., Deuss, A., Van Heijst, H. J. & Woodhouse, J. H. S40RTS: a degree-40 shear-velocity model for the mantle from new Rayleigh wave dispersion, teleseismic traveltime and normal-mode splitting function measurements. *Geophys. J. Int.* **184**, 1223-1236 (2011).

48. Kustowski, B., Ekström, G. & Dziewoński, A. M. Anisotropic shear-wave velocity structure of the Earth's mantle: A global model. *J. Geophys. Res. Solid Earth* **113**, B06306 (2008).

49. Laske, G ., Masters, G ., Ma, Z. & Pasyanos, M. Update on CRUST1.0—a 1-degree global model of Earth's crust. *Geophys. Res. Abstr.* **15**, EGU2013–2658 (2013)

50. Zhang, W. & Shen, W. New estimation of triaxial three-layered Earth's inertia tensor and solutions of Earth rotation normal modes. *Geod. Geodynamics* **11**, 307-315 (2020).

51. Buffett, B. A. Geodynamic estimates of the viscosity of the Earth's inner core. *Nature* **388**, 571-573 (1997).

52. Dumberry, M. Decadal variations in gravity caused by a tilt of the inner core. *Geophys. J. Int.* **172**, 921-933 (2008).

53. Mound, J. E., & Buffett, B. A. Mechanisms of core-mantle angular momentum exchange and the observed spectral properties of torsional oscillations. *J. Geophys. Res. Solid Earth* **110**, B08103 (2005).

54. Mound, J., & Buffett, B. Viscosity of the Earth's fluid core and torsional oscillations. *J. Geophys. Res. Solid Earth* **112**, B05402 (2007).

55. Chao, B. F. Dynamics of the inner core wobble under mantle-inner core gravitational interactions. *J. Geophys. Res. Solid Earth* **122**, 7437-7448 (2017).

56. Chao, B. F. & Shih, S. A. Multipole expansion: unifying formalism for Earth and planetary gravitational dynamics. *Surv. Geophys.* **42**, 803-838 (2021).

57. Rochester, M. G., Crossley, D. J. & Chao, B. F. On the physics of the inner-core

wobble; corrections to "dynamics of the inner-core wobble under mantle-inner-core gravitational interactions" by BF Chao. *J. Geophys. Res. Solid Earth* **123**, 9998-10 (2018).

Acknowledgements

The authors thank B. F. Chao for useful discussion. This study is supported by the National Natural Science Foundation of China (Grants: 42388102, 42192531, and 42192533), the Special Fund of Hubei Luojia Laboratory (grant # 220100002).

Authors contributions

H.D, W.J and J.L supervised the project. Y.A conceived the idea, designed the experiments, conducted the data analysis, comparison, modelling, and wrote the first draft. H.D conducted the data analysis, prepared the figures, assisted in the overall conceptualization and interpretation of results, and contributed substantially to the writing of the manuscript. F.R contributed to data validation, interpretation of results, and the writing of the manuscript. W.J, J.L, and W.S contributed to discussions of the data and analysis and interpretation of results. All authors participated in the writing of the manuscript.

Ethics declarations

Competing interests

The authors declare no competing interests.

Data and materials availability

The ΔLOD and external sources datasets used in this work are available via IERS (https://www.iers.org/IERS/EN/DataProducts/EarthOrientationData/eop.html). The degree-2 order-2 gravitational field Stokes coefficients measured by the SLR and GRACE can be respectively downloaded from https://filedrop.csr.utexas.edu/pub/slr/degree_2/C22_S22_RL06.txt and https://icgem.gfz-potsdam.de/sl/temporal. Hydrological model is from GES DISC (nasa.gov). The mantle's speed models S40RTS and S362MANI are respectively from SubMachine: Web-based tools for exploring seismic tomography and other models of Earth's deep interior (ox.ac.uk) and SAGE: Data Services Products: EMC-S362ANI+M (iris.edu). The test code of the AR-z spectrum has been uploaded to https://agupubs.onlinelibrary.wiley.com/doi/10.1029/2018JB015890. It is also available from the corresponding author H.D upon request.

Extended data figures

Extended Data Fig. 1 to Fig. 4

Supplementary information

This PDF file includes:

Length-of-day variation observation and external excitation sources

Spectra of the degree-2 order-2 gravitational Stokes coefficients

Supplementary Fig.1 to Fig.4